RESEARCH ARTICLE SUMMARY

STRUCTURAL BIOLOGY

Structural insights into ion conduction by channelrhodopsin 2

Oleksandr Volkov,* Kirill Kovalev,* Vitaly Polovinkin,* Valentin Borshchevskiy,* Christian Bamann, Roman Astashkin, Egor Marin, Alexander Popov, Taras Balandin, Dieter Willbold, Georg Büldt, Ernst Bamberg,† Valentin Gordeliy†

INTRODUCTION: Ion channels are integral membrane proteins that upon stimulation modulate the flow of ions across the cell or organelle membrane. The resulting electrical signals are involved in biological functions such as electrochemical transmission and information processing in neurons. Channelrhodopsins (ChRs) appear to be unusual channels. They belong to the large family of microbial rhodopsins, seven-helical transmembrane proteins containing retinal as chromophore. Photon absorption initiates retinal isomerization resulting in a photocycle, with different spectroscopically distinguishable intermediates, thereby controlling the opening and closing of the channel. In 2003, it was demonstrated that light-induced currents by heterologously expressed ChR2 can be used to change a host's membrane potential. The concept was further applied to precisely control muscle and neural activity by using light-induced depolarization to trigger an action potential in neurons expressing ChR2. This optogenetic approach with ChR2 and other ChRs has been widely used for remote control of neural cells in culture and in living animals with high spatiotemporal resolution. It is also used in biomedical studies aimed to cure severe diseases.

RATIONALE: Despite the wealth of biochemical and biophysical data, a high-resolution structure and structural mechanisms of a native ChR2 (and other ChRs) have not yet been known. A step forward was the structure of a chimera (C1C2). However, recent electrophysiological and Fourier transform infrared data showed that C1C2 exhibits light-induced responses that are functionally and mechanistically different from ChR2. Given that ChR2 is the most frequently used tool in optogenetics, a high-resolution structure of ChR2 is of high importance. Deciphering the structure of the native channel would shed light on how the light-induced changes at the retinal Schiff base (RSB) are linked to the channel operation and may make engineering of enhanced optogenetic tools more efficient.

RESULTS: We expressed ChR2 in LEXSY and used in the meso crystallization approach to determine the crystal structure of the wild-type ChR2 and C128T slow mutant at 2.4 and 2.7 Å, respectively (C, cysteine; T, threonine). Two different dark-state conformations of ChR2 in the two protomers in the asymmetric unit were resolved. The overall structure alignment of the protomers does not show a visible difference in backbone conformation. However, the conformation of some amino acids and the position of water molecules are not the same. The dimerization is strong and provided mainly through the interaction of helices 3 and 4 and the N termini. In addition, the protomers are connected with a disulfide bond, C34/C36′. In both protomers, we identified ion conduction pathway comprising four cavities [extracellular cavity 1 (EC1), EC2, intracellular cavity 1 (IC1), and IC2] that are separated by three gates [extracellular gate (ECG), central gate (CG), and intracellular gate (ICG)] (figure, panel A). Arginines R120 and R268 are the cores of ECG and ICG, respectively, in all ChRs. The Schiff base is hydrogen-bond–connected to E123 and D253 amino acids (E, glutamic acid; D, aspartic acid) and is a key part of the CG that is further connected with two other gates through an extended H-bond network mediated by numerous water molecules (figure, panel B). The DC gate is separate from the gates in the channel pathway and is bridged by hydrogen bonds through the water molecule w5. Hydrogen bonding of the DC pair (C128 and D156) has two important consequences. It stabilizes helices 3 and 4 and provides connection from D156, a possible proton donor, to the RSB. The presence of the hydrogen bonds provides structural insights into how the DC gate controls ChR2 gating lifetime.

ON OUR WEBSITE

Read the full article at http://dx.doi.org/10.1126/science.aan8862

CONCLUSION: The determined structures of ChR2 and its C128T mutant present the molecular basis for the understanding of ChR functioning. They provide insights into mechanisms of channel opening and closing. A plausible scenario is that the disruption of the H-bonds between E123 and D253 and the Schiff base and the protonation of D253 upon retinal isomerization trigger rearrangements in the extended hydrogen-bonded networks, stabilizing the ECG and CG and also rearranging the H-bonding network in the cavities. Upon retinal isomerization, these two gates are opened and the network is broken. This leads to the reorientation of helix 2. Additional changes in helices 6 and 7 induced by the isomerization could help with opening the ICG and channel pore formation. ■

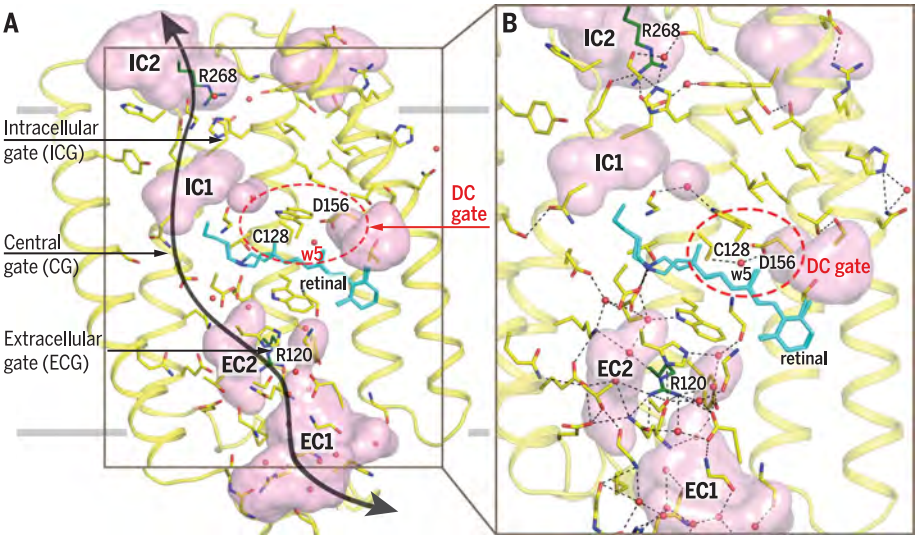

General structure presentation of ChR2. (**A**) Four cavities and three gates forming the channel pore. (**B**) Extended hydrogen-bond network. The DC gate is shown in the red ellipse. The black arrows and gray horizontal lines show the putative ion pathway and position of hydrophobic/hydrophilic boundaries, respectively.

The list of author affiliations is available in the full article online.
*These authors contributed equally to this work.
†Corresponding author. Email: ernst.bamberg@biophys.mpg.de (E.B.); valentin.gordeliy@ibs.fr (V.G.)
Cite this article as O. Volkov *et al.*, *Science* **358**, eaan8862 (2017). DOI: 10.1126/science.aan8862

RESEARCH ARTICLE

STRUCTURAL BIOLOGY

Structural insights into ion conduction by channelrhodopsin 2

Oleksandr Volkov,[1]* Kirill Kovalev,[1,2,3,4]* Vitaly Polovinkin,[1,2,3,5]* Valentin Borshchevskiy,[3]* Christian Bamann,[6] Roman Astashkin,[2,3] Egor Marin,[3] Alexander Popov,[7] Taras Balandin,[1] Dieter Willbold,[1,2,8] Georg Büldt,[3] Ernst Bamberg,[6]† Valentin Gordeliy[1,2,3]†

The light-gated ion channel channelrhodopsin 2 (ChR2) from *Chlamydomonas reinhardtii* is a major optogenetic tool. Photon absorption starts a well-characterized photocycle, but the structural basis for the regulation of channel opening remains unclear. We present high-resolution structures of ChR2 and the C128T mutant, which has a markedly increased open-state lifetime. The structure reveals two cavities on the intracellular side and two cavities on the extracellular side. They are connected by extended hydrogen-bonding networks involving water molecules and side-chain residues. Central is the retinal Schiff base that controls and synchronizes three gates that separate the cavities. Separate from this network is the DC gate that comprises a water-mediated bond between C128 and D156 and interacts directly with the retinal Schiff base. Comparison with the C128T structure reveals a direct connection of the DC gate to the central gate and suggests how the gating mechanism is affected by subtle tuning of the Schiff base's interactions.

Introduction

Ion channels are integral membrane proteins that upon stimulation (for example, with voltage, temperature, ligands such as second messengers, or mechanical stress) modulate the flow of ions across the cell or organelle membrane (*1*). The resulting electrical signals are involved in biological functions such as electrochemical transmission and information processing in neurons. The first light-gated ion channels, channelrhodopsin 1 (ChR1) and ChR2 from the alga *Chlamydomonas reinhardtii*, were discovered and characterized in 2002 and 2003 (*2*, *3*). ChRs are photoreceptors that mediate phototaxis (*4*). They belong to the large family of microbial rhodopsins, seven-helical transmembrane (TM) proteins containing retinal as a cofactor covalently attached to a lysine residue via a protonated Schiff base (RSBH+) (*5*). Photon absorption catalyzes retinal isomerization, which triggers a series of functional and structural transformations in the protein that are correlated with spectral changes (*6*). Other family members are light-driven proton, anion, or cation pumps, or photoreceptors (*6*).

In 2003, it was demonstrated that light-induced currents by heterologously expressed ChR2 can be used to change a host's membrane potential (*3*). The concept was further applied to precisely control muscle and neural activity by using light-induced depolarization to trigger an action potential in neurons expressing ChR2 (*7*, *8*). This optogenetic approach with ChR2 and other newly discovered ChRs has been widely used for remote control of neural cells in culture tissue and in living animals with high spatiotemporal resolution in a cell-specific manner (*9*). It has also been used in biomedical treatments aimed to restore vision (*10*) or hearing (*11*).

A high-resolution structure of the native ChR2 has not yet been known. A step forward was made when the structure of a chimera (C1C2), consisting of the first five TM helices of ChR1 and the last two TMs of ChR2, was solved (*12*, *13*). As a light-gated cation channel, ChR1 shares many properties with ChR2 (*2*), and both have a high sequence identity in the TM part (65%). However, recent electrophysiological and Fourier transform infrared (FTIR) spectroscopy data showed that C1C2 exhibits light-induced responses that are functionally and mechanistically different from ChR2 (*14*). Given that ChR2 is the most used tool in optogenetics, a high-resolution structure of ChR2 is of high interest (*15*).

Like other microbial rhodopsins, ChR2 undergoes a photocycle with spectrally distinct intermediates starting with the retinal isomerization from the all-*trans* to 13-*cis* (P_1^{500}) state. The RSBH+ is stabilized by two acidic counterions (E123 and D253), and isomerization disturbs the network, leading to deprotonation (P_2^{390}) and reprotonation (P_3^{520}) reactions at the RSB. The amino acid sequence has common features with light-driven proton pumps like bacteriorhodopsin (BR) and other microbial rhodopsins, and the photocycle manifests proton transfer reactions (*16*). However, ChR2 acts as a leaky pump, where cations can permeate decoupled from the reactions at the RSB during the photocycle (*17*). This cation pathway closes upon the decay of the P_3^{520} state, which is followed by a P_4^{480} state that lasts for seconds. In the transition from the closed state to the open state, further structural changes take place like a pronounced movement of helix 2 and water entry into the protein (*15*). However, the linkage between all these light-induced changes and the open channel are still under debate, which is further complicated by the requirement of at least two closed states and two photoreactions to describe the electrophysiological data (*18*).

Here, we present x-ray crystallographic structures of the wild-type ChR2 and its slow C128T mutant (solved to 2.39- and 2.7-Å resolution, respectively), indicating that the rhodopsin-derived channels are different from other ion channels. The structure of ChR2 also exhibits considerable differences from the C1C2 chimera: (i) ChR2 has two conformations in the ground state; (ii) there are additional gates in the extracellular and intracellular parts of the protein; and (iii) there is a water-mediated hydrogen bond between C128 and D156 explaining the mechanism of DC gating. These and other features of the structures give insight into the molecular mechanism of ChR2 and other ChRs.

Overall ChR2 structure

We obtained two crystal forms for both ChR2 and the C128T mutant that were expressed in *Leishmania tarentolae* (fig. S1): one hexagonal-shaped and the other rod-shaped (fig. S2), which was the one to determine the structure of ChR2 at 2.39 Å and the structure of the C128T mutant at 2.7 Å, respectively (table S1). All the crystals belong to type I (characterized by layer-like packing of the crystals), and the protein packing is membrane-like as usual in the case of in meso grown crystals (fig. S3). It is the first example of a membrane protein crystal structure using this organism as the expression host. Figure 1 (A to C) displays the overall structure of the C-terminally truncated protein comprising amino acids 1 to 315. We observe a dimer with similar arrangements of the seven TMs in each protomer as in a 6-Å structure from cryo–electron microscopy (EM) (*19*). At the extracellular side, the N termini of both protomers form a domain stabilized by two disulfide bridges. The seven TMs are connected by short loops and a β sheet (residues 107 to 117) between TM2 and TM3. In the middle of the membrane, the retinal chromophore separates ChR2 into an intracellular side and an extracellular side. A continuous channel pore cannot be seen in our closed-state structure, but as outlined in more detail below, we can identify four cavities that are separated by constrictions that we term gates in the following (Fig. 2A): close to

[1]Institute of Complex Systems (ICS), ICS-6: Structural Biochemistry, Research Centre Juelich, Juelich, Germany. [2]Institut de Biologie Structurale Jean-Pierre Ebel, Université Grenoble Alpes–Commissariat à l'Energie Atomique et aux Energies Alternatives–CNRS, Grenoble, France. [3]Moscow Institute of Physics and Technology, Dolgoprudny, Russia. [4]Institute of Crystallography, University of Aachen, Aachen, Germany. [5]ELI Beamlines, Institute of Physics, Czech Academy of Sciences, 18221 Prague, Czech Republic. [6]Max Planck Institute of Biophysics, Frankfurt am Main, Germany. [7]European Synchrotron Radiation Facility, 38027 Grenoble, France. [8]Institut für Physikalische Biologie, Heinrich-Heine-Universität Düsseldorf, Düsseldorf, Germany.
*These authors contributed equally to this work.
†Corresponding author. Email: ernst.bamberg@biophys.mpg.de (E.B.); valentin.gordeliy@ibs.fr (V.G.)

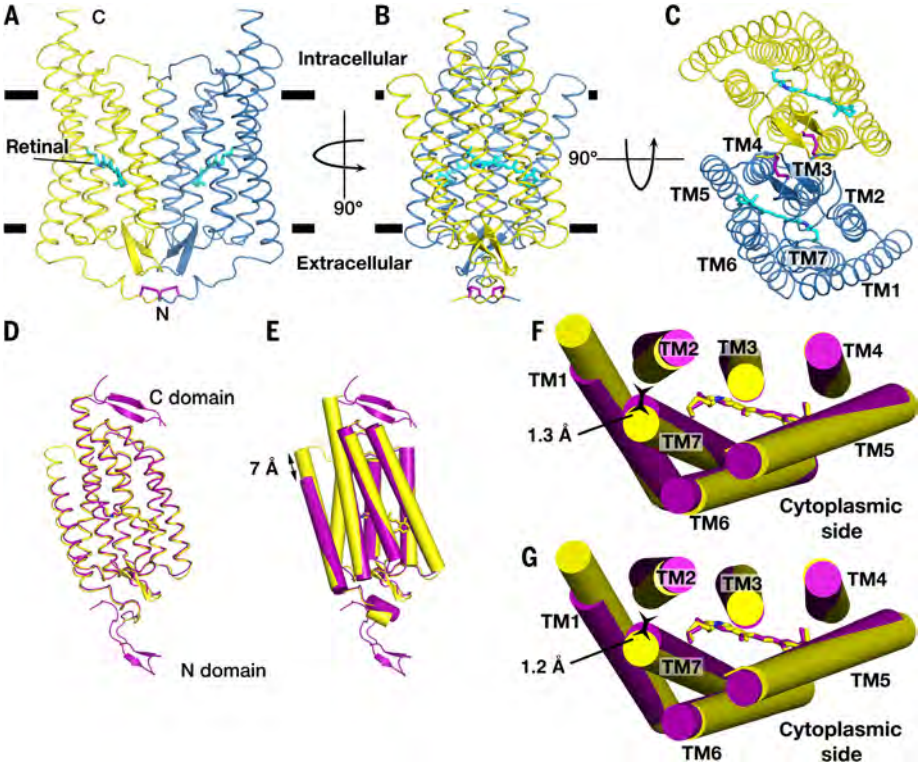

Fig. 1. General structure of ChR2 and its alignment with the C1C2 structure. (**A** to **C**) Overall structure presentation of the ChR2 dimer. Cysteine bridges are shown in purple. (**D** to **G**) Overall structure comparison of ChR2 (yellow) and the chimera C1C2 (purple). (D to F) Comparison performed by overall alignment of two structures. (G) Comparison performed using TM6 and TM7 alignment of two structures. The C1C2 model was taken from the PDB (ID 3UG9). The hydrophobic membrane core boundaries were calculated using the PPM server (*56*) and are shown by the black lines.

the retinal is the central gate (CG); walking along the membrane normal to the intracellular side, we find CG connected to intracellular cavity 1 (IC1), followed by the intracellular gate (ICG) and intracellular cavity 2 (IC2), which is connected to the intracellular side. Moving toward the extracellular side, the CG connects first to extracellular cavity 2 (EC2), followed by the extracellular gate (ECG) and extracellular cavity 1 (EC1). The DC gate, which is named after D156 in TM4 and C128 in TM3 (*15*) and is conserved in many ChRs (fig. S4A), is located close to the RSBH+ and not in the putative ion pore. Still, it has a strong effect on the open channel lifetime.

We observe two different dark-state conformations of ChR2 in the two protomers in the asymmetric unit. The protomers interact through helices TM5 and TM5′, which are oriented in opposite directions with hydrogen bonds between Y172/N187′ and N187/Y172′ (fig. S5B). Cysteines C183/C183′ are 3.5 Å apart, which is not close enough to create a disulfide bridge between the helices. The overall structure alignment of the protomers does not show a visible difference in backbone conformation (fig. S6A). However, the conformation of some amino acids and the position of water molecules are not the same. In particular, the intracellular amino acid S155 hydrogen bonds with T188 in the case of protomer A, whereas in protomer B, S155 flips to hydrogen bond with N187 (fig. S6B). A similar flexibility has also been observed in simulations with a ChR2 model (*20*). In addition, the water molecule w4, present in protomer A, is missing in protomer B, and the water molecules w2 and w3 have different positions. This results in differences in the extended hydrogen-bond networks in the RSB and the proton acceptor D253 environment (fig. S6C) of the extracellular part of ChR2. Nevertheless, we will use only protomer A in those discussions where the differences in the protomers are insignificant.

The dimerization is provided mainly through the interaction of helices 3 and 4 and the N termini (fig. S7). In the intracellular part of the protein, the following pairs of amino acids are hydrogen-bonded: Y145/Y145′ of TM4/TM4′, Y184/Y85′ of TM5/TM2′; V154 of TM4 is connected with Y85′ of TM2′ through w19 and with L125′ and L126′ of TM3′ through w18/w19. Nearly all these amino acids are conserved in all ChRs (fig. S4A). In the extracellular part, hydrogen bonding between the protomers in the dimer is provided by the following pairs: W118/T165′ of TM3/TM4′ and A111′/Y109 of the loops connecting TM2′-TM3′ and TM2-TM3, respectively. The amino acids are highly conserved among all ChRs (fig. S4A). In addition, the protomers are connected with the disulfide bond C34/C36′. The connection between the dimers is strong. Electron paramagnetic resonance (EPR) spectroscopy studies show that breaking the disulfide bond between C34 and C36 by double mutation is not sufficient to prevent the dimerization (*21*, *22*).

In Fig. 1 (D to G), we show an overall structure comparison of ChR2 and the chimera C1C2. The alignment of the structures shows considerable differences between the two proteins. There are differences in the length and orientation of the helices. Helix 1 is 7 Å longer in ChR2 model. Several helices deviate more than 1 Å in length (for instance, for TM7, it is 1.3 Å; Fig. 1F). Such differences result in different hydrogen-bond patterns, intra- and interhelical interactions, and residue conformations. Together, these lead to different geometry and properties of the channel. We also illustrate the differences by aligning the proteins relative to helices 6 and 7, which are the same in both proteins. However, both helices in the chimera structure still deviate from the ones in ChR2 (Fig. 1G). One more distinct difference between the chimera and ChR2 structures is that C1C2 shows considerably fewer internal water molecules. Thus, the C1C2 structure differs considerably from ChR2 despite a high conservation of key amino acids.

Structure of the retinal pocket

The retinal isomer composition of ChR2 dark state(s) was determined by different methods. Retinal extraction and Raman spectroscopy showed a mixture of 70:30% all-*trans*, 15-*anti* and 13-*cis*, 15-*syn* (*23*, *24*), whereas solid-state nuclear magnetic resonance spectroscopy demonstrated the presence of 100% all-*trans* isomer (*25*). Therefore, we used both isomer ratios to refine the crystallographic data. The mixture of conformations fits well the electron densities of the retinal pocket (Fig. 3, A and B) and preserves the salt bridge between the RSBH+ and its counterion complex E123/D253 (Fig. 3A). The presence of either two or only one retinal conformation(s) does not result in any visible differences in the structure of the retinal pocket. The retinal is attached to the conserved lysine K257 residue. In contrast to BR, the protonated RSB (RSBH+) of ChR2 is not stabilized by a water molecule, but it is in direct contact with its counterion complex E123 and D253 [the analogs of D85 and D212 in BR (*26*); fig. S4B]. Both residues have been suggested to act as proton acceptors of the RSBH+ during the photocycle (*27*, *28*). The oxygen atoms of these residues are at distances of 2.8 and 3.2 Å from RSB. E123 is further connected to T127 (with a hydrogen bond of 3.0 Å) and to the water molecules w1 and w2. D253 also interacts with K93 and with w1 and w2 through two hydrogen bonds. In its turn, w1 is connected with another key amino acid, E90, and w2 is connected to the water molecule w3 and W124 (Fig. 3A). An extended hydrogen-bond network interconnects D253 and E123 with E90, K93, E97, W124, T127, and P227 through w1, w2, w3, w4, and w6 (Figs. 3 and 4). The RSB, the proton acceptor D253, and E90 build up the CG together with S63 and N258, whereas the water molecules w1 to w4 make a connection to the ECG, with

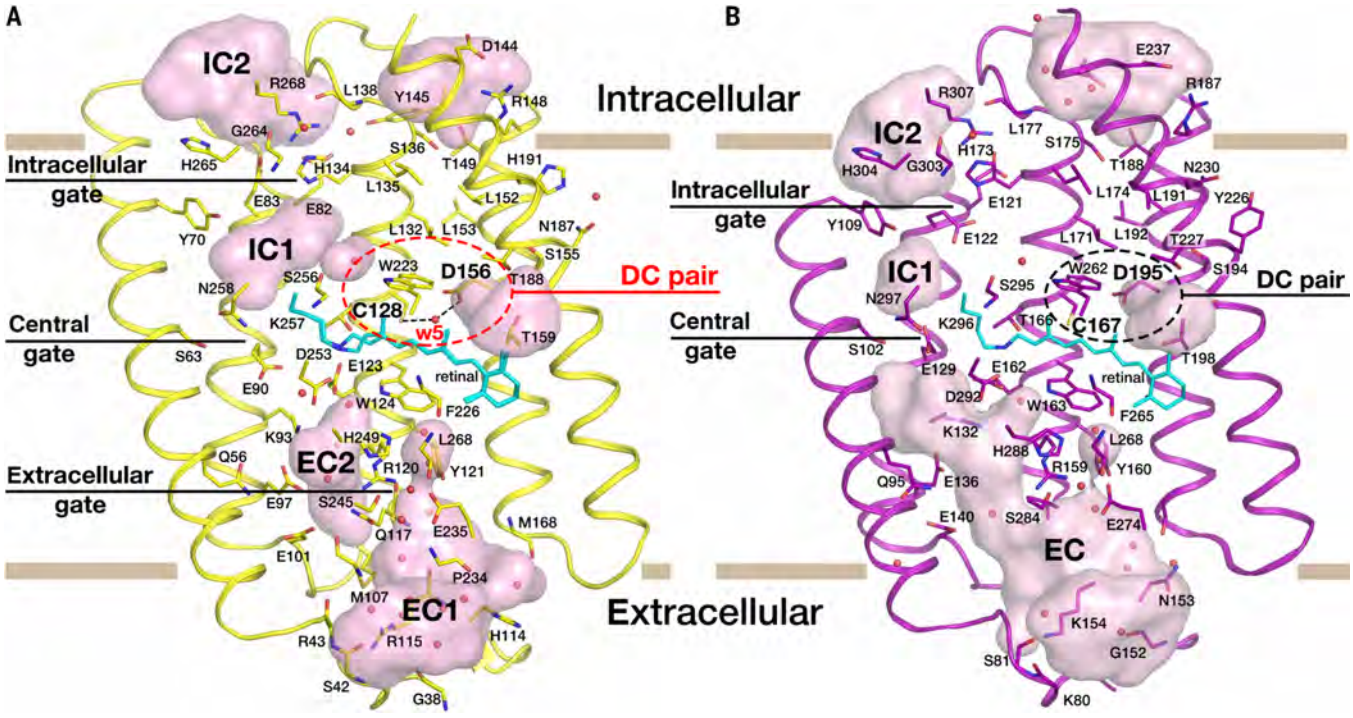

Fig. 2. Cavities and highly conserved amino acids of ChR2 and C1C2. (**A**) Protomer A of ChR2 and the four main cavities: EC1, EC2, IC1, and IC2. DC pair is shown in the red ellipse together with the water molecule w5. (**B**) C1C2 structure. DC pair, which lacks the water molecule, is shown in the black ellipse. The cavities were calculated using HOLLOW (*57*). TM6 and TM7 helices are not shown. The hydrophobic membrane core boundaries are shown by the gray lines. Single-letter abbreviations for the amino acid residues are as follows: A, Ala; C, Cys; D, Asp; E, Glu; F, Phe; G, Gly; H, His; I, Ile; K, Lys; L, Leu; M, Met; N, Asn; P, Pro; Q, Gln; R, Arg; S, Ser; T, Thr; V, Val; W, Trp; and Y, Tyr.

R120 in the center (see below). Figure 3 (B and C) shows the views to the CG along the channel from the EC2 and IC1, respectively. We suggest that when the Schiff base isomerizes and D253 accepts the proton (*28*), D253 rearrangements destroy the existing hydrogen-bond network extending to R120 and E90. This likely results in the rearrangement of E90, R120, and D253, which, in turn, boosts a synchronized opening of the ECG and CG. The conformational changes may also initiate the opening of the CG from the extracellular part of the channel. This is supported by the fact that three of the abovementioned amino acids (K93, E97, and T127) are highly conserved among ChRs, and R120, D253, E90, W124, and P227 are completely conserved in ChRs (fig. S4A). In addition, E97, R120, and D253 are among the five known residues, for which mutations lead to an almost complete cessation of the photocurrents in all the tested ChR variants (*15*).

Figure S8 (A and B) compares the retinal pockets in ChR2 and the chimera C1C2. In ChR2, E90 is a key determinant of ion selectivity (*29*, *30*), and the corresponding amino acid E129 of C1C2 is not hydrogen-bonded to the proton acceptor D292 (corresponding to D253 in ChR2; Fig. 3). Hence, it cannot directly be influenced by retinal isomerization and the subsequent protonation of D292. This difference explains recent FTIR spectroscopy data showing that, upon continuous illumination, C1C2 exhibits structural changes distinct from those in ChR2 and, in particular, the protonation of E129 is not changed as in the case of E90 of ChR2 (*14*)

Numerous previous studies on ChR2 show the key amino acids involved in cation channeling (*15*, *18*). They are distributed along the cavities and gates discussed below, and therefore, we suggest that the ions move through four large cavities (EC1, EC2, IC1, and IC2) (Fig. 2) only when all three gates (ECG, CG, and ICG) are open at the same time. This raises the following questions: (i) How is the opening and closing of the gates controlled? (ii) How is the opening and closing of different gates synchronized? (iii) How do the gates protect the channel pathway against leakage? To answer these questions, we will discuss in detail the structure of the gates and cavities.

Interaction of the RSBH+ with the gates in the channel pore formed by four cavities

All the cavities in ChR2, except the one in the vicinity of the retinal's β-ionone ring, are highly hydrophilic. In Fig. 2, we compare the differences to the C1C2 chimera, where only some of the cavities and vestibules have been described (*13*). In C1C2, the extracellular vestibule extends continuously from the extracellular part nearly to the vicinity of the Schiff base (fig. S9) and has been suggested to be an extracellular ion pathway (*13*). In contrast, in ChR2, the cation pathway consists of two cavities (EC1 and EC2), which are separated by the ECG. At its center, the gate contains the conserved arginine R120, a key amino acid in all microbial rhodopsins.

A large cavity (IC1) in the intracellular part of the protein is surrounded by residues Y70, E83, E82, K257, and N258. It extends nearly to the DC gate (Fig. 2A), in contrast to the smaller cavity found in C1C2 (Fig. 2B). IC1 of ChR2 is separated from the EC2 by the CG comprising residues S63, E90, D253, and N258. IC1 is not in direct contact with the cytoplasm, but it is separated from another IC2 by the ICG that comprises the residues Y70, E82, E83, H134, H265, and R268 (Fig. 2A). A similar gate was identified in C1C2, but it comprises only two amino acids, Y109 and E122 (Fig. 2B).

As noted above, the extracellular part of the channel of ChR2 is not continuous but is blocked by constriction sites presented by the ECG and CG (Figs. 2 and 4). The ECG of ChR2 comprises M107, Q117, Y121, W124, S245, and H249, with R120 in the center (Fig. 4, A and B). There is an extended hydrogen-bond network connecting all these amino acids. The network comprises five water molecules, w6 to w10, of EC1 and three water molecules, w2 to w4, of EC2. R120 is in the core of the gate and is H-bonded to all of the gating amino acids and also to D253. The water molecules w1 to w4 of EC2 connect the gate with the proton acceptor D253 and with Q56, E90, K93, E97, E101, and E123 that surround the cavity EC2 from the CG side. The ECG and CG are connected to each other through E90 that is hydrogen-bonded through w1 to K93, E123, and

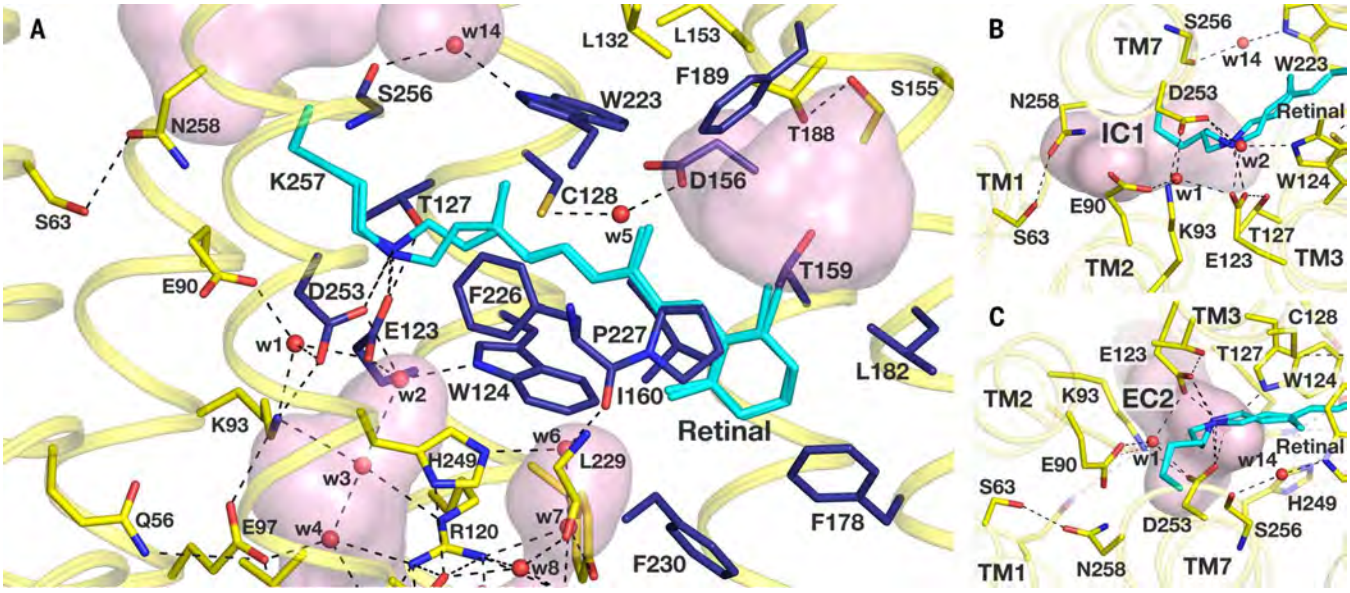

Fig. 3. Retinal pocket and CG of ChR2. (**A**) Protomer A of ChR2. Residues forming retinal binding pocket are shown in dark blue. TM5 and TM6 helices are not shown. Retinal is colored cyan. (**B**) View of IC1 from CG. (**C**) View of EC from CG.

D253 (Fig. 4A). This residue is a key determinant of ion selectivity, and its replacement with a positively charged residue (lysine or arginine) inverts the ChR2 selectivity to anions like chloride (*29*). Hence, in the open state, E90 is in a position to interact with the permeating cations and to affect ion selectivity (*29*, *30*). We further suggest that R120 plays a central role in the channel opening, consistent with its known significance in other microbial rhodopsins (*31*). A plausible scenario is that the disruption of the H-bonds between E123 and D253 and the Schiff base and the protonation of D253 upon retinal isomerization (*28*) trigger rearrangements in the hydrogen-bonded networks stabilizing the ECG and CG and also rearranging the H-bonding network in the cavities. The structure explains why E97A, R120A, and D253A/N mutations in ChRs lead to an almost complete cessation of the photocurrents (*2*, *32*, *33*). These residues are needed to sustain a stable network for the extended cavities in the open state. Starting with the events at the RSBH+, this leads to the synchronized opening of the ECG and CG. The gating amino acids Y121, R120, W124, S245, and H249 and Q56, E90, K93, E97, E101, M107, and E123 that block the cavity EC2 from the extracellular and intracellular sides, respectively, are highly conserved (fig. S4A), suggesting that the structural organization of the channel pathway and the mechanism of channel operation at the ECG are common for most of the known ChRs.

The extracellular ion channel pathway extends to the intracellular side through two additional cavities (IC1 and IC2) of ChR2 (fig. S10). The large cavity IC1 starts from the CG (starting from the vicinity of E90) to the cavity IC2, which is connected directly to the cytoplasm. Between the cavities IC1 and IC2, there is the ICG (Figs. 2 and 5A). As noted above, E90 is downshifted from IC2 to the EC2 and, unlike in C1C2, it is not connected to N258 (fig. S11). The ICG is composed of the conserved residues Y70, E82, E83, H134, G234, H265, and R268 interconnected by hydrogen bonds partially mediated by w16. All these amino acids are conserved in known ChRs (fig. S4A), and H134D and H265R mutations led to a nearly complete cessation of the photocurrents (*2*, *32*, *33*). How is the ICG opened? One possible scenario is as follows. The amino acids E90, K93, E97, E101, and M107 are interconnected via a hydrogen-bond network with the ECs, ECG, and the retinal pocket (Figs. 3 and 4). We note that four of these residues are on the same side of helix 2, and therefore, the H-bond network strongly contributes to the stabilization of the helix (Fig. 4). Upon retinal isomerization, the CG and ECG are opened and the network is broken. This leads to the reorientation of helix 2, as has been observed by EPR and EM studies of the structure of the open channel in light-activated ChR2 (*21*, *22*, *34*). Additional changes in helices 6 and 7 induced by the isomerization (*21*, *34*) could help to open the ICG by changing the position of R268 in the open state. R268 forms a salt bridge with E82 and E83; the reorientation of the helices opens the pathway from the cytoplasmic side (Fig. 5), and the ICG is open. Parts of the suggested mechanism have been described before based on FTIR data and simulations on a ChR2 model (*27*).

The DC gate and its interaction with the Schiff base

The DC gate is separate from the previous gates that are located in the channel pore. Mutations in the DC gate strongly alter the gating kinetics and extend the lifetime of the conducting state 10^2- to 10^5-fold (*35*, *36*), but the nature of the DC gate is still under debate. Our ChR2 structure shows that the DC gate consists of C128 and D156 bridged by hydrogen bonds through the water molecule w5 (Figs. 2 to 4). The hydrogen bond of D156 was assigned in data from infrared spectroscopy (*37*), although C128 was considered to be the direct hydrogen-bonding partner. However, a water-mediated hydrogen bond between C128 and D156 was suggested before in a computational model (*20*). The important water molecule was not detected in the C1C2 structure. The presence of the DC motif has two important consequences. The first is the stabilization of helices 3 and 4, and the second is the connection from D156 to the RSB. Data from infrared spectroscopy assigned D156 as the proton donor to the deprotonated RSB in the P_2^{390} state (*28*). This is consistent with the D156A phenotype, which is similar to proton donor mutants in BR. It accumulates a long-lasting P_2^{390} state, with a deprotonated RSB that retards the channel-closing reaction by several orders of magnitude (*35*). The structure of ChR2 provides additional support for the hypothesis that D156 may be a proton donor. Although the distance from the RSB to C128 is too large for a direct proton transfer from the DC gate, an additional residue, T127, may facilitate reprotonation of the Schiff base. This amino acid is conserved in most ChRs or substituted by serine. In the ChR2 ground state, T127 forms a hydrogen bond to E123 that we suggest is broken upon light activation. The subsequent rearrangement may result in the creation of a hydrogen bond between T127 and the Schiff base. The sensitivity of T127's hydrogen-bonding pattern to the protonation state of the counterion was recently also described in computer simulations (*20*). It seems to be an interesting link between the RSB and the DC gate.

To better understand the DC gate, we solved the structure of the slow C128T mutant. Overall, structural alignment does not display visible differences between ChR2 and the mutant (Fig. 6A). However, there are three regions of the proteins where local structures are different (Fig. 6, B to D). First, the hydrogen bonding of T128 and D156 is preserved, but it is not mediated by a

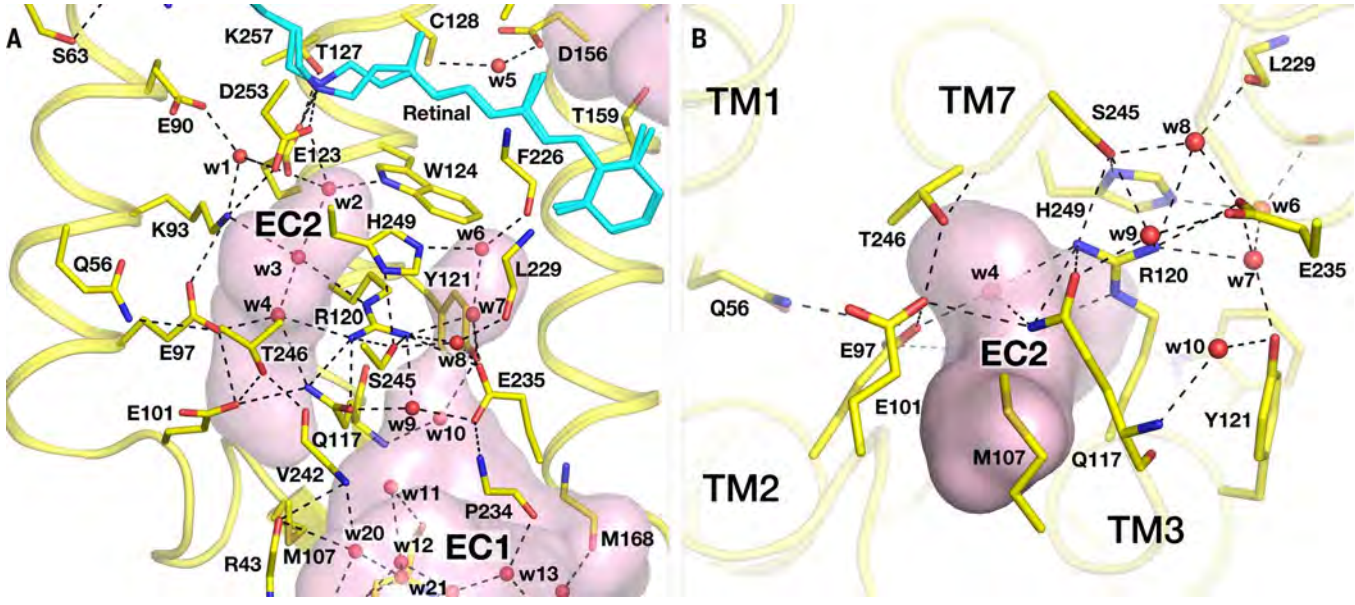

Fig. 4. ECG and its interaction with the retinal pocket. (**A**) Protomer A of ChR2. TM6 and TM7 helices are not shown. (**B**) View of EC2 from ECG.

water molecule as in ChR2; rather, the amino acids are directly connected by a hydrogen bond (Fig. 6B and fig. S12). This bonding is confirmed by infrared spectroscopy data of the wild-type ChR2 and the C128T mutant. The frequency shift seen in the mutant suggests that D156 forms a stronger hydrogen bond in the dark in the wild-type ChR2 (*37*). The C128T mutant also has a prolonged open-state lifetime but a different photochemistry than the D156A mutant. The reprotonation is not directly rate-limiting for channel closure because C128T also accumulates an intermediate with an RSBH+ (P_3^{520}). Here, we speculate that the tuning of the interaction between helices 3 and 4 or the modification of the network to other gates is responsible for the slow mutant phenotype. The mutation also disturbs the structure of the retinal pocket. The distance between T127 and T128 is 0.7 Å longer than that between T127 and C128. In C128T, the length of the hydrogen bond between T127 and E123 is increased from 2.9 to 3.2 Å and, between E123 and the Schiff base, from 2.6 to 3.1 Å. There are also conformational differences in the region of CG and ECG (Fig. 6, C and D). Water molecules w1 to w4 are not at the same positions. Moreover, the mutation results in an additional water molecule, w2″, in the region of w2, and E90 is no longer H-bonded with E123 (Fig. 6C). Another significant difference is that the mutation destroys direct H-bond connection between K93 and E97.

Many of the residues in the gates have only a modest effect on the gating kinetics and often a weak phenotype upon mutation. This is different for the DC gate. Our structure reveals the proton pathway that connects D156 with the CG and the RSB. Both intermediates (P_2^{390} and P_3^{520}) are present in the open state, whereas the transition to the open state is mainly followed by helix hydration caused by water influx (*38*). To prevent the possible blockage of the channel by the RSBH+ in the open state, either the proton of the RSB is transferred to the acceptor (P_2^{390}) or RSBH+ points toward the cytoplasmic side due to stabilization by the now deprotonated D156 (P_3^{520}). Upon reisomerization to the all-*trans* isomer upon P_3^{520} decay, the RSBH+ will block cation permeation and start to reestablish the interaction networks with other gates. Some of the latter processes can take tens of seconds, for example, the reprotonation of E90 or the reversal of the global changes in TM2 (*27*, *28*, *39*). Thus, mutations that affect the stabilization of the deprotonated RSB or the RSBH+ by the deprotonated D156 in the open state will control the gating kinetics for the channel. In D156A, the proton donor is missing and P_2^{390} is accumulated. In contrast, fast reprotonation can be observed in the C128T mutant, but the deprotonated D156 is stabilized in a different interaction network so that it is not getting reprotonated on the wild type's time scale in milliseconds.

ChR2 must have evolved a pathway used for the reprotonation of D156. At the cytoplasmic side, we identify a hydrophilic vestibule involving the charged residues D144, R148, and E198. It extends in the direction of the DC gate toward the conserved amino acids S136 and T149 (figs. S12 and S13A). Proton transfer from the intracellular side to D156 is prevented by a highly hydrophobic region comprising four conserved residues: L132, L135, L152, and L153 (figs. S4A and S12 to S14). Such a structural arrangement is similar to BR. Here, the protonation of the RSB from the proton donor D96 is prevented in the dark state by a similar leucine barrier (figs. S4A, S13, and S14). D96 is hydrogen-bonded to T46 and has a similar distance to the RSB as the hydrogen-bonded S136 and T149 to D156 in ChR2 (fig. S14, A and B). To reprotonate D96, the proton has to overcome the same leucine barrier and the same distance through a proton wire in the N-to-O transition of BR's photocycle (fig. S14, A and B) (*26*, *40*). We suggest that the cavity, together with the residues S136 and T149 and the region composed of L132, L135, L152, and L153, may define the intracellular part of the proton uptake pathway for D156 (fig. S13A). We speculate that not only does the hydrogen bond between C128 and D156 of the DC gate stabilize helices 3 and 4 but also the hydrogen bond between the pair S136 and T149 may play an important role in the channel and pumping properties of ChR2. Both pairs connect helices 3 and 4 where the leucine residues in the hydrophobic barrier are located (L132 and L135 in helix 3 and L152 and L153 in helix 4). In ChR2, as in BR, reprotonation of the RSB (by D96 in BR and D156 in ChR2) may trigger the opening of the proton pathway for proton uptake from the cytoplasm (*41*, *42*). However, deprotonation of D156 may be insufficient to reorganize the hydrophobic gate between D156 and cytoplasm, and the breakage of the S136-T149 hydrogen bond may facilitate proton transfer to the deprotonated D156. This reprotonation of D156 and the rearrangements of hydrogen bonds connecting helices 3 and 4 may be a determinant of channel closing (fig. S15). We cannot exclude an alternative pathway through H191 and N187 (fig. S14). In the asymmetric unit, the conserved S155 is connected to either N187 or T188, which is close to D156.

The interaction network of RSBH+ and its involvement in the gating reaction have been addressed before in computer simulations of ChR2 homology models (*20*, *27*). There is a striking consistency for several aspects and interpretations, for example, the conformational heterogeneity of S155, the water molecule w5 in the DC gate (*20*), or the destabilization of TM2 upon

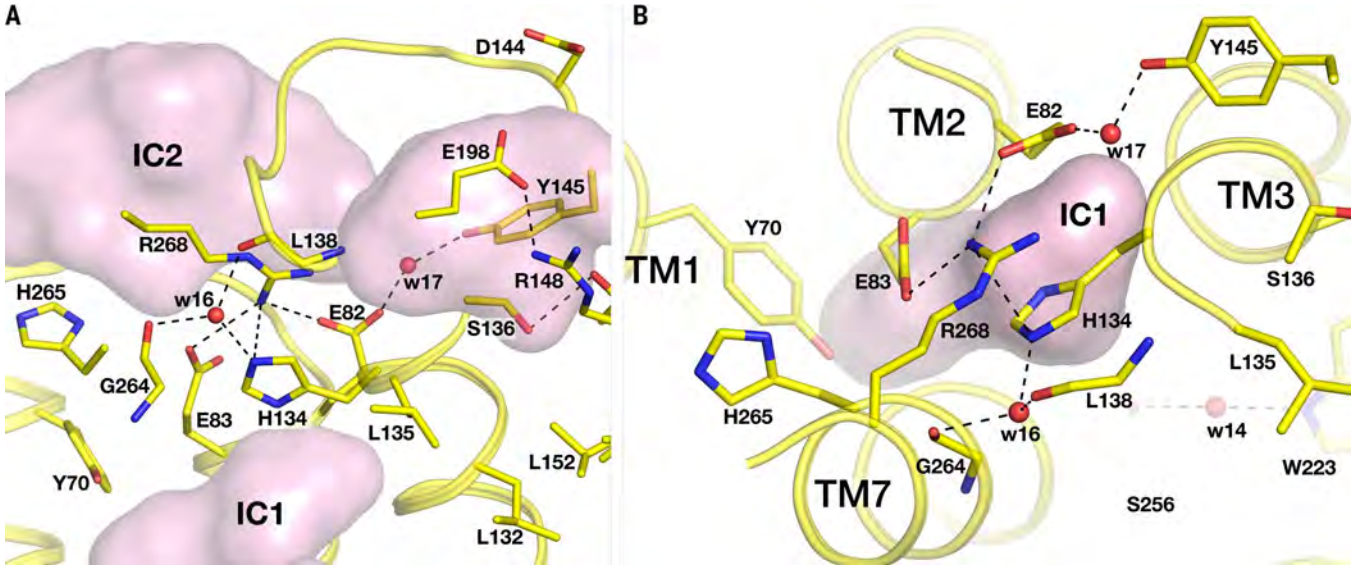

Fig. 5. Intracellular gate. (**A**) Structure of protomer A in the ChR2 dimer model. TM6 and TM7 helices are not shown. (**B**) View of IC1 from ICG.

isomerization (*27*). However, our structural model still has unique features, especially the arrangement of the counterion, the water molecules, and the interaction of E90. Aside from the different conformations of S155, we do not observe other regions with such heterogeneity but cannot rule it out for the retinal isomer composition. It is an attractive idea to consider the two dark closed-state conformations as a basis to explain the electrophysiological data that require two closed and two conductive states (*43*, *44*), and further simulations with our model as a starting point will help to clarify this important topic.

In ChR2, the cavities are formed by extended interaction networks comprising hydrophilic side chains and water molecules, a feature that is reminiscent of the light-driven proton pump BR. Presumably, ChRs evolved from a common ancestor together with the light-driven proton pumps by increasing the cavities' volume (fig. S13). Changes in the network of a proton pumping rhodopsin led to an increased water mobility and turned the pump into a proton channel (*45*). Hence, subtle modification in the network and especially an increase in the number of water molecules and their dynamics might be key properties in light-gated ion channels. The transition to the open channel is best reflected in spectral markers for helix hydration that correlates with the kinetics of conductivity changes. The water influx is needed for cation permeation (*38*). The presented structures, together with the analysis of spectroscopic and physiological data, provide a first insight into the mechanisms of native light-gated channels and a molecular basis for a rational design of new optogenetic tools.

Materials and methods

Sequence alignment

For sequence alignment (fig. S4a) we used: ChR2 from *Chlamydomonas reinhardtii* (UniProt ID: Q8RUT8), ChR1 from *Chlamydomonas reinhardtii* (UniProt ID: Q93WP2), VChR1 from *Volvox carteri* (UniProt ID: B4Y103), VChR2 from *Volvox carteri* (UniProt ID: B4Y105), Crimson from *Chlamydomonas nostigama* (NCBI ID: KF992060), Chronos from *Stigeoclonium helveticum* (NCBI ID: KF992040), TsChR from *Tetraselmis striata* (NCBI ID: KF992089), PsChR from *Platymonas subcordiformus* (NCBI ID: JX983143), NsChR from *Neochlorosarcina* (NCBI ID: KF992054), SdChR from *Scherffelia dubia* (NCBI ID: KF992072), BsChR1 from *Brachiomonas submarina* (NCBI ID: KF992086), BsChR2 from *Brachiomonas submarina* (NCBI ID: KF992034), HdChR from *Haematococcus droebakensis* (NCBI ID: KF992059), TcChR from *Tetraselmis cordiformis* (NCBI ID: KF992057), CoChR from *Chloromonas oogama* (NCBI ID: KF992041), CsChR from *Chloromonas subdivisa* (NCBI ID: KF992078), CnChR2 from *Chlamydomonas noctigama* (NCBI ID: KF992073), AgChR from *Asteromonas gracilis-B* (NCBI ID: KF992038), CbChR1 from *Chlamydomonas bilatus-A* (NCBI ID: KF992062), DChR1 from *Dunaliella salina* (NCBI ID: JQ241364). The C-termini of all presented channel rhodopsins are truncated. The alignment was done with Unipro UGENE software using Clustal Omega algorithm.

The sequence alignment between ChR2, bacteriorhodopsin (PDB ID: 1IW6), proteorhodopsin (PDB ID: 4HYJ), halorhodopsin (PDB ID: 1E12), sensory rhodopsin II (PDB ID: 3QAP) and light-driven sodium pump (PDB ID: 4XTL) was created based on secondary structure matching (SSM) superposition, using the PDBeFold server (fig. S4b).

For sequence alignments visualization ESPript3.0 server was used (*46*).

Protein expression and purification

The gene encoding ChR2 (1–315 aa) from *Chlamydomonas reinhardtii* (UniProt Q8RUT8) was synthesized de novo. The nucleotide sequence was optimized for *Leishmania tarentolae* expression with the GeneOptimizer software (Thermo Fisher Scientific). C128T and N24Q mutations were introduced into this gene by PCR. Both genes in fusion with the C-terminal polyhistidine tags (H9) were introduced into the integrative inducible expression vector pLEXSY_I-blecherry3 (Jena Bioscience, Germany) through the BglII and NotI restriction sites.

The *Leishmania tarentolae* cells of the strain LEXSY host T7-TR (Jena Bioscience) were transformed with the ChR2 expression plasmid linearized by the SwaI restriction enzyme. After the clonal selection, the transformed cells were grown at 26°C in the dark in shaking baffled flasks in the Brain-Heart-Infusion Broth (Carl Roth, Germany) supplemented with 5 μg/ml Hemin, 50 U/ml penicillin and 50 μg/ml streptomycin (both antibiotics from AppliChem). When OD_{600} = 1 was reached, 5 μM all-trans-retinal (Sigma-Aldrich) and 10 μg/ml tetracycline were added, and incubation continued for further 24h. The collected cells were disrupted in an M-110P Lab Homogenizer (Microfluidics) at 10,000 psi in a buffer containing 50 mM NaH_2PO_4/Na_2HPO_4, pH 7.6, 0.2 M NaCl, 10% glycerol, 1 mM EDTA, 2 mM 6-aminohexanoic acid (AppliChem), 50 mg/L DNase I (Sigma-Aldrich) and cOmplete protease inhibitor cocktail (Roche). The membrane fraction of the cell lysate was isolated by ultracentrifugation at 120,000g for 1h at 4°C. The pellet was resuspended in the same buffer but without DNase I and stirred for 1h at 4°C. The ultracentrifugation step was repeated again. Finally, the membranes were resuspended in the solubilization buffer containing 20 mM HEPES, pH 8.0, 0.2 M NaCl, cOmplete, 1% DDM (Cube Biotech), 5 μM all-trans-retinal and stirred overnight for solubilization (*47*). The insoluble fraction was removed by ultracentrifugation at 120,000g for 1h at 4°C. The supernatant was loaded on an Ni-NTA resin (Cube Biotech), and ChR2 was eluted in a buffer containing 20 mM

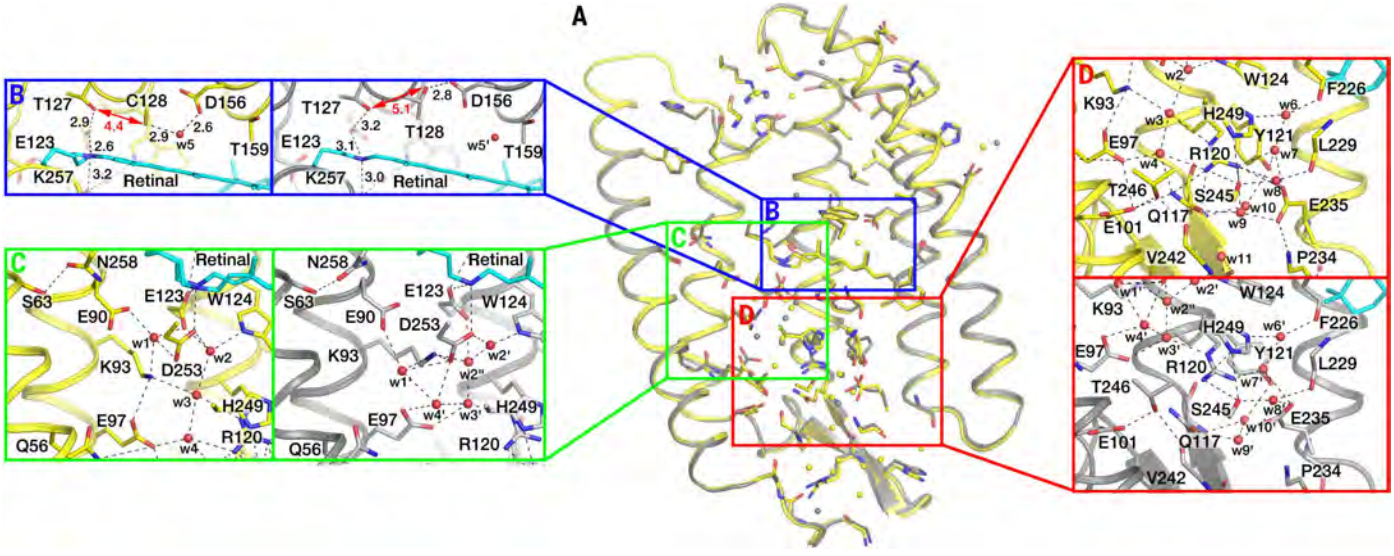

Fig. 6. Comparison of the structures of ChR2 and C128T mutant. (**A**) Overall alignment of wild-type and mutant structures. (**B**) Detailed comparison of DC gate region, (**C**) active center and CG, and (**D**) ECG.

HEPES, pH 7.5, 0.2 M NaCl, 0.2 M L-Histidine (AppliChem), 2 mM 6-aminohexanoic acid, cOmplete, and 0.1% DDM. The eluate was subjected to size-exclusion chromatography on a Superdex 200 Increase 10/300 GL column (GE Healthcare Life Sciences) in a buffer containing 50 mM NaH_2PO4/Na_2HPO4, pH 5.2, 0.2 M NaCl, 1 mM EDTA, 2 mM 6-aminohexanoic acid, cOmplete and 0.05% DDM. Protein-containing fractions with an A280/A470 absorbance ratio of ~1.8 were pooled and concentrated to 40 mg/ml for crystallization.

Crystallization

The crystals were grown with an in meso approach (*48*, *49*), similar to that used in our previous work (*50*). The solubilized protein in the crystallization buffer was mixed with premelted at 42°C monoolein (Nu-Chek Prep) to form a lipidic mesophase. 300 nl aliquots of a protein–mesophase mixture were spotted on a 96-well LCP glass sandwich plate (Marienfeld) and overlaid with 500 nL of precipitant solution by means of the NT8 crystallization robot (Formulatrix). The best crystals of both wild-type ChR2 and C128T mutant were obtained with a protein concentration of 30 mg/ml and 0.6 M KH_2PO_4/Na_2HPO_4, pH 5.2-5.6. The crystals were grown at 22°C and reached the final size within 2 to 6 months. The hexagonal-shaped crystal and rod-shaped crystals grew to 30–40 μm and 50–150 μm in size, respectively (fig. S2). Before harvesting, the crystals were incubated for 5 min in cryoprotectant solution (2.4 M KH_2PO_4/Na_2HPO_4, pH 5.2-5.6, 20% (w/v) glycerol). All crystals were harvested using micromounts (MiTeGen), and were flash-cooled and stored in liquid nitrogen.

Collection and treatment of diffraction data

X-ray diffraction data for native and mutant protein were collected at ID30B, ID23-1 and ID29 ESRF at 100 K with a PILATUS 6M (Dectris) detector. Diffraction images were processed with XDS (*51*). XSCALE (*51*) was used to merge 11 and 2 data sets together for native and mutant protein, respectively. PHENIX was used to convert intensities to structure factor amplitudes and generate Rfree labels (*52*).

Structure solution and refinement

The native protein structure was phased by molecular replacement in PHASER (*53*) with 3UG9 (*13*) followed by PHENIX AutoBuild (*52*). The initial model was iteratively refined using Coot (*54*) and REFMAC5 (*55*). The structure of mutant ChR2 was obtained by refinement of the native protein.

REFERENCES AND NOTES

1. K. S. Cole, R. F. Baker, Longitudinal impedance of the squid giant axon. *J. Gen. Physiol.* **24**, 771–788 (1941). doi: 10.1085/jgp.24.6.771; pmid: 19873252
2. G. Nagel *et al*., Channelrhodopsin-1: A light-gated proton channel in green algae. *Science* **296**, 2395–2398 (2002). doi: 10.1126/science.1072068; pmid: 12089443
3. G. Nagel *et al*., Channelrhodopsin-2, a directly light-gated cation-selective membrane channel. *Proc. Natl. Acad. Sci. U.S.A.* **100**, 13940–13945 (2003). doi: 10.1073/pnas.1936192100; pmid: 14615590
4. O. A. Sineshchekov, K.-H. Jung, J. L. Spudich, Two rhodopsins mediate phototaxis to low- and high-intensity light in *Chlamydomonas reinhardtii*. *Proc. Natl. Acad. Sci. U.S.A.* **99**, 8689–8694 (2002). doi: 10.1073/pnas.122243399; pmid: 12060707
5. D. Oesterhelt, W. Stoeckenius, Rhodopsin-like protein from the purple membrane of Halobacterium halobium. *Nat. New Biol.* **233**, 149–152 (1971). doi: 10.1038/newbio233149a0; pmid: 4940442
6. O. P. Ernst *et al*., Microbial and animal rhodopsins: Structures, functions, and molecular mechanisms. *Chem. Rev.* **114**, 126–163 (2014). doi: 10.1021/cr4003769; pmid: 24364740
7. X. Li *et al*., Fast noninvasive activation and inhibition of neural and network activity by vertebrate rhodopsin and green algae channelrhodopsin. *Proc. Natl. Acad. Sci. U.S.A.* **102**, 17816–17821 (2005). doi: 10.1073/pnas.0509030102
8. G. Nagel *et al*., Light activation of channelrhodopsin-2 in excitable cells of *Caenorhabditis elegans* triggers rapid behavioral responses. *Curr. Biol.* **15**, 2279–2284 (2005). doi: 10.1016/j.cub.2005.11.032; pmid: 16360690
9. L. Fenno, O. Yizhar, K. Deisseroth, The development and application of optogenetics. *Annu. Rev. Neurosci.* **34**, 389–412 (2011). doi: 10.1146/annurev-neuro-061010-113817; pmid: 21692661
10. H. P. N. Scholl *et al*., Emerging therapies for inherited retinal degeneration. *Sci. Transl. Med.* **8**, 368rv6 (2016). doi: 10.1126/scitranslmed.aaf2838; pmid: 27928030
11. T. Moser, Optogenetic stimulation of the auditory pathway for research and future prosthetics. *Curr. Opin. Neurobiol.* **34**, 29–36 (2015). doi: 10.1016/j.conb.2015.01.004; pmid: 25637880
12. H. E. Kato, O. Nureki, Crystal structure of channelrhodopsin, a light-gated cation channel—All cations lead through the monomer. *Biophysics* **9**, 57–61 (2013). doi: 10.2142/biophysics.9.57; pmid: 27493541
13. H. E. Kato *et al*., Crystal structure of the channelrhodopsin light-gated cation channel. *Nature* **482**, 369–374 (2012). doi: 10.1038/nature10870; pmid: 22266941
14. A. Inaguma *et al*., Chimeras of channelrhodopsin-1 and -2 from *Chlamydomonas reinhardtii* exhibit distinctive light-induced structural changes from channelrhodopsin-2. *J. Biol. Chem.* **290**, 11623–11634 (2015). doi: 10.1074/jbc.M115.642256; pmid: 25796616
15. V. A. Lórenz-Fonfría, J. Heberle, Channelrhodopsin unchained: Structure and mechanism of a light-gated cation channel. *Biochim. Biophys. Acta* **1837**, 626–642 (2014). doi: 10.1016/j.bbabio.2013.10.014; pmid: 24212055
16. M. Nack *et al*., Kinetics of proton release and uptake by channelrhodopsin-2. *FEBS Lett.* **586**, 1344–1348 (2012). doi: 10.1016/j.febslet.2012.03.047; pmid: 22504075
17. K. Feldbauer *et al*., Channelrhodopsin-2 is a leaky proton pump. *Proc. Natl. Acad. Sci. U.S.A.* **106**, 12317–12322 (2009). doi: 10.1073/pnas.0905852106; pmid: 19590013
18. F. Schneider, C. Grimm, P. Hegemann, Biophysics of channelrhodopsin. *Annu. Rev. Biophys.* **44**, 167–186 (2015). doi: 10.1146/annurev-biophys-060414-034014; pmid: 26098512
19. M. Müller, C. Bamann, E. Bamberg, W. Kühlbrandt, Projection structure of channelrhodopsin-2 at 6 Å resolution by electron crystallography. *J. Mol. Biol.* **414**, 86–95 (2011). doi: 10.1016/j.jmb.2011.09.049; pmid: 22001017
20. H. C. Watanabe, K. Welke, D. J. Sindhikara, P. Hegemann, M. Elstner, Towards an understanding of channelrhodopsin function: Simulations lead to novel insights of the channel mechanism. *J. Mol. Biol.* **425**, 1795–1814 (2013). doi: 10.1016/j.jmb.2013.01.033; pmid: 23376098
21. N. Krause, C. Engelhard, J. Heberle, R. Schlesinger, R. Bittl, Structural differences between the closed and open states of channelrhodopsin-2 as observed by EPR spectroscopy. *FEBS Lett.* **587**, 3309–3313 (2013). doi: 10.1016/j.febslet.2013.08.043; pmid: 24036447

22. T. Sattig, C. Rickert, E. Bamberg, H.-J. Steinhoff, C. Bamann, Light-induced movement of the transmembrane helix B in channelrhodopsin-2. *Angew. Chem. Int. Ed.* **52**, 9705–9708 (2013). doi: 10.1002/anie.201301698; pmid: 23893661
23. M. Nack, I. Radu, C. Bamann, E. Bamberg, J. Heberle, The retinal structure of channelrhodopsin-2 assessed by resonance Raman spectroscopy. *FEBS Lett.* **583**, 3676–3680 (2009). doi: 10.1016/j.febslet.2009.10.052; pmid: 19854176
24. E. Ritter, P. Piwowarski, P. Hegemann, F. J. Bartl, Light-dark adaptation of channelrhodopsin C128T mutant. *J. Biol. Chem.* **288**, 10451–10458 (2013). doi: 10.1074/jbc.M112.446427; pmid: 23439646
25. J. Becker-Baldus *et al*., Enlightening the photoactive site of channelrhodopsin-2 by DNP-enhanced solid-state NMR spectroscopy. *Proc. Natl. Acad. Sci. U.S.A.* **112**, 9896–9901 (2015). doi: 10.1073/pnas.1507713112; pmid: 26216996
26. D. Bashford, K. Gerwert, Electrostatic calculations of the pK_a values of ionizable groups in bacteriorhodopsin. *J. Mol. Biol.* **224**, 473–486 (1992). doi: 10.1016/0022-2836(92)91009-E; pmid: 1313886
27. J. Kuhne *et al*., Early formation of the ion-conducting pore in channelrhodopsin-2. *Angew. Chem. Int. Ed.* **54**, 4953–4957 (2015). doi: 10.1002/anie.201410180; pmid: 25537168
28. V. A. Lórenz-Fonfría *et al*., Transient protonation changes in channelrhodopsin-2 and their relevance to channel gating. *Proc. Natl. Acad. Sci. U.S.A.* **110**, E1273–E1281 (2013). doi: 10.1073/pnas.1219502110; pmid: 23509282
29. J. Wietek *et al*., Conversion of channelrhodopsin into a light-gated chloride channel. *Science* **344**, 409–412 (2014). doi: 10.1126/science.1249375
30. K. Eisenhauer *et al*., In channelrhodopsin-2 glu-90 is crucial for ion selectivity and is deprotonated during the photocycle. *J. Biol. Chem.* **287**, 6904–6911 (2012). doi: 10.1074/jbc.M111.327700; pmid: 22219197
31. K. Gerwert, E. Freier, S. Wolf, The role of protein-bound water molecules in microbial rhodopsins. *Biochim. Biophys. Acta* **1837**, 606–613 (2014). doi: 10.1016/j.bbabio.2013.09.006; pmid: 24055285
32. A. P. Plazzo *et al*., Bioinformatic and mutational analysis of channelrhodopsin-2 protein cation-conducting pathway. *J. Biol. Chem.* **287**, 4818–4825 (2012). doi: 10.1074/jbc.M111.326207; pmid: 22139833
33. Y. Sugiyama *et al*., Photocurrent attenuation by a single polar-to-nonpolar point mutation of channelrhodopsin-2. *Photochem. Photobiol. Sci.* **8**, 328–336 (2009). doi: 10.1039/b815762f; pmid: 19255673
34. M. Müller, C. Bamann, E. Bamberg, W. Kühlbrandt, Light-induced helix movements in channelrhodopsin-2. *J. Mol. Biol.* **427**, 341–349 (2015). doi: 10.1016/j.jmb.2014.11.004; pmid: 25451024
35. C. Bamann, R. Gueta, S. Kleinlogel, G. Nagel, E. Bamberg, Structural guidance of the photocycle of channelrhodopsin-2 by an interhelical hydrogen bond. *Biochemistry* **49**, 267–278 (2010). doi: 10.1021/bi901634p; pmid: 20000562
36. A. Berndt, O. Yizhar, L. A. Gunaydin, P. Hegemann, K. Deisseroth, Bi-stable neural state switches. *Nat. Neurosci.* **12**, 229–234 (2009). doi: 10.1038/nn.2247; pmid: 19079251
37. M. Nack *et al*., The DC gate in Channelrhodopsin-2: Crucial hydrogen bonding interaction between C128 and D156. *Photochem. Photobiol. Sci.* **9**, 194 (2010). doi: 10.1039/b9pp00157c; pmid: 20126794
38. V. A. Lórenz-Fonfría *et al*., Temporal evolution of helix hydration in a light-gated ion channel correlates with ion conductance. *Proc. Natl. Acad. Sci. U.S.A.* **112**, E5796–E5804 (2015). doi: 10.1073/pnas.1511462112; pmid: 26460012
39. E. Ritter, K. Stehfest, A. Berndt, P. Hegemann, F. J. Bartl, Monitoring light-induced structural changes of channelrhodopsin-2 by UV-visible and Fourier transform infrared spectroscopy. *J. Biol. Chem.* **283**, 35033–35041 (2008). doi: 10.1074/jbc.M806353200; pmid: 18927082
40. S. Wolf, E. Freier, M. Potschies, E. Hofmann, K. Gerwert, Directional proton transfer in membrane proteins achieved through protonated protein-bound water molecules: A proton diode. *Angew. Chem. Int. Ed.* **49**, 6889–6893 (2010). doi: 10.1002/anie.201001243; pmid: 20680951
41. E. Freier, S. Wolf, K. Gerwert, Proton transfer via a transient linear water-molecule chain in a membrane protein. *Proc. Natl. Acad. Sci. U.S.A.* **108**, 11435–11439 (2011). doi: 10.1073/pnas.1104735108; pmid: 21709261
42. T. Wang *et al*., Deprotonation of D96 in bacteriorhodopsin opens the proton uptake pathway. *Structure* **21**, 290–297 (2013). doi: 10.1016/j.str.2012.12.018; pmid: 23394942
43. K. Stehfest, P. Hegemann, Evolution of the channelrhodopsin photocycle model. *ChemPhysChem* **11**, 1120–1126 (2010). doi: 10.1002/cphc.200900980; pmid: 20349494
44. K. Nikolic *et al*., Photocycles of channelrhodopsin-2. *Photochem. Photobiol.* **85**, 400–411 (2009). doi: 10.1111/j.1751-1097.2008.00460.x; pmid: 19161406
45. A. Vogt *et al*., Conversion of a light-driven proton pump into a light-gated ion channel. *Sci. Rep.* **5**, 16450 (2015). doi: 10.1038/srep16450; pmid: 26597707
46. X. Robert, P. Gouet, Deciphering key features in protein structures with the new ENDscript server. *Nucleic Acids Res.* **42**, W320–W324 (2014). doi: 10.1093/nar/gku316; pmid: 24753421
47. C. Bamann, T. Kirsch, G. Nagel, E. Bamberg, Spectral characteristics of the photocycle of channelrhodopsin-2 and its implication for channel function. *J. Mol. Biol.* **375**, 686–694 (2008). doi: 10.1016/j.jmb.2007.10.072; pmid: 18037436
48. V. I. Gordeliy, R. Schlesinger, R. Efremov, G. Büldt, J. Heberle, Crystallization in lipidic cubic phases: A case study with bacteriorhodopsin. *Membr. Protein Protoc.* **228**, 305–316 (2003). doi: 10.1385/1-59259-400-X:305; pmid: 12824562
49. V. I. Gordeliy *et al*., Molecular basis of transmembrane signalling by sensory rhodopsin II–transducer complex. *Nature* **419**, 484–487 (2002). doi: 10.1038/nature01109; pmid: 12368857
50. I. Gushchin *et al*., Crystal structure of a light-driven sodium pump. *Nat. Struct. Mol. Biol.* **22**, 390–395 (2015). doi: 10.1038/nsmb.3002; pmid: 25849142
51. W. Kabsch, XDS. *Acta Crystallogr. D Biol. Crystallogr.* **66**, 125–132 (2010). doi: 10.1107/S0907444909047337; pmid: 20124692
52. P. D. Adams *et al*., PHENIX: A comprehensive Python-based system for macromolecular structure solution. *Acta Crystallogr. D Biol. Crystallogr.* **66**, 213–221 (2010). doi: 10.1107/S0907444909052925; pmid: 20124702
53. A. J. McCoy *et al*., Phaser crystallographic software. *J. Appl. Crystallogr.* **40**, 658–674 (2007). doi: 10.1107/S0021889807021206; pmid: 19461840
54. P. Emsley, K. Cowtan, *Coot*: Model-building tools for molecular graphics. *Acta Crystallogr. D Struct. Biol.* **60**, 2126–2132 (2004). doi: 10.1107/S0907444904019158; pmid: 15572765
55. G. N. Murshudov *et al*., REFMAC5 for the refinement of macromolecular crystal structures. *Acta Crystallogr. D Biol. Crystallogr.* **67**, 355–367 (2011). doi: 10.1107/S0907444911001314; pmid: 21460454
56. M. A. Lomize, I. D. Pogozheva, H. Joo, H. I. Mosberg, A. L. Lomize, OPM database and PPM web server: Resources for positioning of proteins in membranes. *Nucleic Acids Res.* **40**, D370–D376 (2012). doi: 10.1093/nar/gkr703; pmid: 21890895
57. B. K. Ho, F. Gruswitz, HOLLOW: Generating accurate representations of channel and interior surfaces in molecular structures. *BMC Struct. Biol.* **8**, 49 (2008). doi: 10.1186/1472-6807-8-49; pmid: 19014592

ACKNOWLEDGMENTS

We are grateful to M. Michel for the idea on the choice of the best suitable expression system. We thank A. Yuzhakova, D. Volkov, and C. Baeken for technical assistance with protein production. We acknowledge the Structural Biology Group of European Synchrotron Radiation Facility for granting access to the synchrotron beamlines and for assistance with data collection. The work was supported by the common program of Agence Nationale de la Recherche (France) and Deutsche Forschungsgemeinschaft (Germany) (ANR-15-CE11-0029-02) and CEA(IBS)-HGF(FZJ) STC 5.1 specific agreement. Crystallization, x-ray data collection and treatment, as well as data analysis and manuscript preparation were supported by the Russian Science Foundation (16-15-00242). The work used the platforms of the Grenoble Instruct Centre (ISBG; UMS 3518 CNRS-CEA-UJF-EMBL) with support from the French Infrastructure for Integrated Structural Biology (FRISBI; ANR-10-INSB-05-02) and New Generation of Drugs for Alzheimer's Disease (GRAL; ANR-10-LABX-49-01) within the Grenoble Partnership for Structural Biology (PSB). The work was also supported by ERA.Net RUS Plus (ID 323). V.B. acknowledges the Ministry of Education and Science of the Russian Federation (project no. 6.9909.2017/BY). E.B. and C.B. were supported by the German Research Foundation Collaborative Research Center 807, the Center of Excellence Frankfurt Macromolecular Complexes, and the Max Planck Society. D.W. was supported by the German Research Foundation Collaborative Research Centers 974 and 1208. V.P. also acknowledges the support of the ELIBIO project (CZ.02.1.01/0.0/0.0/15_003/0000447) from the European Regional Development Fund. V.G. designed the project, directed and supervised all the research, and wrote the manuscript with strong contribution from E.B., C.B., K.K., and O.V. and help from all other authors. V.G. and E.B. analyzed the results with contribution from K.K., O.V., G.B., C.B., and D.W. O.V. developed the expression and expressed and purified the proteins with contribution from T.B. V.P. crystallized the protein with contribution from K.K. and O.V. A.P., K.K., V.P., O.V., and R.A. collected the data. V.B., K.K., and E.M. did the crystallographic part of the work. Atomic coordinates and structure factors for the reported crystal structures have been deposited with the Protein Data Bank (PDB) under the accession codes 6EID and 6EIG (wild-type ChR2 and C128T mutant, respectively). All other data to support the conclusions are in the paper or the supplementary materials. The authors declare no competing financial interests.

SUPPLEMENTARY MATERIALS

www.sciencemag.org/content/358/6366/eaan8862/suppl/DC1
Figs. S1 to S15
Table S1

5 June 2017; accepted 30 October 2017
10.1126/science.aan8862

Science

Structural insights into ion conduction by channelrhodopsin 2

Oleksandr Volkov, Kirill Kovalev, Vitaly Polovinkin, Valentin Borshchevskiy, Christian Bamann, Roman Astashkin, Egor Marin, Alexander Popov, Taras Balandin, Dieter Willbold, Georg Büldt, Ernst Bamberg and Valentin Gordeliy

Science **358** (6366), eaan8862.
DOI: 10.1126/science.aan8862

The inner workings of an optogenetic tool

Channelrhodopsins are membrane channel proteins whose gating is controlled by light. In their native setting, they allow green algae to move in response to light. Their expression in neurons allows precise control of neural activity, an approach known as optogenetics. Volkov *et al.* describe the high-resolution structure of channelrhodopsin 2, the most widely used optogenetics tool, as well as the structure of a mutant with a longer open-state lifetime (see the Perspective by Gerwert). Light activation perturbs an intricate hydrogen-bonding network to open the channel. The structures provide a basis for designing better optogenetic tools.

Science, this issue p. 10.1126/science.eaan8862; see also p. 1000